

GT2017-64624

Effect of Internal Crossflow Velocity on Film Cooling Effectiveness – Part II: Compound Angle Shaped Holes

John W. McClintic, Joshua B. Anderson, and David G. Bogard

The University of Texas at Austin
Austin, Texas, USA

Thomas E. Dyson
GE Global Research
Niskayuna, New York, USA

Zachary D. Webster
GE Aviation
Evendale, Ohio, USA

ABSTRACT

In gas turbine engines, film cooling holes are commonly fed with an internal crossflow, the magnitude of which has been shown to have a notable effect on film cooling effectiveness. In Part I of this study, as well as in a few previous studies, the magnitude of internal crossflow velocity was shown to have a substantial effect on film cooling effectiveness of axial shaped holes. There is, however, almost no data available in the literature that shows how internal crossflow affects compound angle shaped film cooling holes. In Part II, film cooling effectiveness, heat transfer coefficient augmentation, and discharge coefficients were measured for a single row of compound angle shaped film cooling holes fed by internal crossflow flowing both in-line and counter to the span-wise direction of coolant injection. The crossflow-to-mainstream velocity ratio was varied from 0.2-0.6 and the injection velocity ratio was varied from 0.2-1.7. It was found that increasing the magnitude of the crossflow velocity generally caused degradation of the film cooling effectiveness, especially for in-line crossflow. An analysis of jet characteristic parameters demonstrated the importance of crossflow effects relative to the effect of varying the film cooling injection rate. Heat transfer coefficient augmentation was found to be primarily dependent on injection rate, although for in-line crossflow, increasing crossflow velocity significantly increased augmentation for certain conditions.

INTRODUCTION

GAS TURBINE FILM COOLING

It is necessary in many applications to introduce active cooling to components in the hot section of gas turbine engines to improve part life and durability. Typical designs often route cool air through internal passages beneath the surface of exposed parts. To further cool the part, film cooling, a process by which the coolant is injected through discrete holes over the surface of the part, is often employed. A successful film cooling scheme will produce a thin layer of cool air that protects the surface from the hot overflowing mainstream gas. The film cooling and internal cooling work together to minimize the surface

temperature of the part, which is often normalized as an overall cooling effectiveness:

$$\varphi \equiv \frac{T_\infty - T_m}{T_\infty - T_c} \quad (1)$$

It is often useful, however, to isolate the effects of film cooling. Film cooling is typically evaluated by how it affects the heat transfer into the external surface by altering the driving temperature for heat transfer, T_{aw} , and the heat transfer coefficient, h_f . These parameters are normalized as film cooling effectiveness (or adiabatic effectiveness):

$$\eta \equiv \frac{T_\infty - T_{aw}}{T_\infty - T_{c,exit}} \quad (2)$$

and heat transfer coefficient augmentation, which is the ratio of the external heat transfer coefficients with and without film cooling: h_f/h_0 . Internal cooling can also be characterized by a driving temperature and heat transfer coefficient, T_c and h_c respectively, although for simple internal geometries, these are easier to predict.

A one-dimensional model can be used to demonstrate how internal cooling and external film cooling contribute to the overall film cooling effectiveness:

$$q_f'' = h_f(T_{aw} - T_m) = \frac{T_m - T_c}{t/k - 1/h_c} \quad (3)$$

$$\varphi = \frac{1 - \chi\eta}{1 + Bi + h_f/h_c} + \chi\eta \quad (4)$$

where:

$$\chi \equiv \frac{T_\infty - T_{c,exit}}{T_\infty - T_c} \quad (5)$$

$$Bi \equiv \frac{h_f t}{k} \quad (6)$$

Performing an analysis of this sort allows separate measurements of film cooling effectiveness and heat transfer coefficient augmentation to be combined into a single metric that approximates the ultimate design parameter.

COMPOUND ANGLE SHAPED HOLES

Shaped film cooling holes, or holes with a diffused exit, are commonly featured in the literature and have been consistently shown to improve film cooling effectiveness relative to cylindrical holes. The overwhelming focus of the literature on shaped holes has been directed towards axial shaped holes, and rightly so, given the widespread use of that geometry. Only a few studies have tested shaped holes with a compound injection angle. Introducing a compound injection angle is often necessary in high curvature regions of turbine airfoils to avoid too steep of an injection angle, which degrades film cooling performance [1]. A study by Taslim and Khanicheh [2] found that compound angle shaped holes improved adiabatic effectiveness relative to compound angle cylindrical holes. Bell *et al* [3] tested compound angle fan-shaped holes along with a number of other geometries, including axial shaped holes and found that relative to the other geometries, the compound angle shaped holes had both higher laterally averaged effectiveness and heat transfer coefficient augmentation. They used the net heat flux reduction analysis to show that the compound angle fan-shaped holes performed better than other holes. Ganzert *et al* [4] performed experiments on the suction side of a model turbine blade with axial and compound angle shaped holes and concluded that the compound angle shaped holes caused greater aerodynamic losses due to increased mixing with the mainstream. They also found that heat transfer coefficient augmentation was greater for the compound angle holes than for the axial holes.

INTERNAL CROSSFLOW EFFECTS

The literature shows that the internal geometry supplying coolant to film cooling holes can have an appreciable effect on the film cooling effectiveness. Notable among these is a series of studies at Universität Karlsruhe, including Gritsch *et al* [5] and Saumweber and Schulz [6] who studied the effects of feeding axial fan-shaped and laidback fan-shaped film cooling holes with an internal crossflow, or internal flow oriented perpendicular to the overflowing mainstream, a common internal feed orientation for gas turbine blades. These studies showed that internal crossflow had a strong and detrimental effect relative to feeding axial shaped film cooling holes with a quiescent plenum. This result was also observed by Wilkes *et al* [7], who showed that the internal crossflow-to-mainstream velocity ratio, VR_c , had an appreciable effect on effectiveness while the crossflow Reynolds number had little effect. That work was furthered in Part I of this study [8], which tested a wide range of internal crossflow velocity ratios and jet-to-mainstream velocity ratios, VR . It was found that much of the crossflow effect for axial shaped holes scaled with the hole inlet velocity ratio, $VR_i = U_i/U_j$ (which is matched if both VR and VR_c are also matched).

The effect of internal crossflow was first studied for compound angle round holes by McClintic *et al* [9]. The

direction of internal crossflow was shown to be important for compound angle holes – holes fed by a crossflow directed counter to the spanwise direction of coolant injection had significantly greater effectiveness than holes with crossflow directed in-line with the direction of coolant injection. Stratton *et al* [10] performed a computational study for the same geometry and conditions as [9]. The LES model used by that study produced effectiveness results that reasonably matched the experimental data. It further predicted that the internal crossflow caused a strong swirling within the hole that affected the velocity distribution at the hole exit.

To the authors' knowledge, only one study in the literature has examined the effect of feeding compound angle shaped holes with an internal crossflow. Dittmar *et al* [11] injected coolant from a number of different film cooling hole shapes, including compound angle fan-shaped holes, onto a convex surface approximating the shape of a blade suction surface. They found that directing crossflow in-line with the span-wise direction of coolant produced the highest levels of adiabatic effectiveness. The results for heat transfer coefficient augmentation were mixed and subject to the coolant injection rate. No information regarding the internal crossflow velocity was provided, and only one internal crossflow velocity was tested.

PRESENT STUDY

The literature provides no data concerning the effect of internal crossflow velocity on the film cooling performance of compound angle shaped holes. In this study discharge coefficients, adiabatic effectiveness, and heat transfer coefficient augmentation were measured using a single row of compound angle, shaped holes (using the open literature 7-7-7 geometry). A range of crossflow-to-mainstream velocity ratios of $VR_c = 0.2\text{--}0.6$ was tested at jet-to-mainstream velocity ratios of $VR = 0.2\text{--}1.7$ (a similar range was tested for axial 7-7-7 holes in Part I.). The effect of internal crossflow direction was also studied.

NOMENCLATURE

Bi	Biot number
C_d	discharge coefficient
d	film cooling hole diameter
d_H	hydraulic diameter
DR	density ratio ρ_c/ρ_∞
f	friction factor for Gnielinski's formula
H	boundary layer shape factor
h	heat transfer coefficient
k	thermal conductivity
L	film cooling hole length
M	blowing ratio $\rho_j U_j / \rho_\infty U_\infty$
Nu	Nusselt number
p	film cooling hole pitch, pressure
Pr	Prandtl number
q''	heat flux
R	ideal gas constant for air
r_x	extraction ratio
Re	Reynolds number
t	wall thickness

T	temperature
T_u	turbulence intensity $\sqrt{u'^2}/\bar{U}$
U	velocity
VR	velocity ratio (without subscript: U_j/U_∞)
W	jet width
x	stream-wise coordinate measured from streamwise position of the hole geometric centerline
y	wall-normal coordinate measured from the wall
z	span-wise coordinate

GREEK

α	cooling hole injection angle
β	cooling hole lateral expansion angle
δ	boundary layer thickness, uncertainty
δ^*	boundary layer displacement thickness
ε	compound injection angle
φ	overall cooling effectiveness
γ	specific heat ratio, forward expansion angle
η	adiabatic effectiveness
Λ_x	turbulence integral length scale
θ	normalized temperature, boundary layer momentum thickness
ρ	density
χ	coolant warming factor

SUBSCRIPTS, ACCENTS

aw	adiabatic wall
b	bias uncertainty
c	coolant, crossflow
CL	centerline
f	with film cooling
i	hole inlet
j	coolant jet
m	metal
p	precision uncertainty
t	total pressure/temperature
0	without film cooling
∞	mainstream
$-$	laterally averaged

EXPERIMENTAL FACILITIES AND PROCEDURES

DESCRIPTION OF FACILITIES

Experiments were performed at the University of Texas at Austin in a low speed, low temperature, recirculating wind tunnel. Anderson *et al* [12] and Wilkes *et al* [7] provide a detailed description of the facility. The test section was configured to provide flow over a flat plate and enabled control of the mainstream turbulence and the approach boundary layer characteristics. Figure 1 shows a side-view schematic of the test section, which features an upstream passive turbulence generator, a suction slot to remove the upstream boundary layer, and a cylindrical boundary layer trip, 3.175 mm in diameter, positioned 108mm upstream of $x = 0$. The mainstream flow

parameters were held constant for all conditions tested and are given in Table 1 below.

Cool air was supplied to the film cooling holes through a channel mounted below the test plate and oriented perpendicular to the main flow loop. The flow in the channel was fully developed turbulent internal flow. Cross-sectional dimensions of the channel are shown in Figure 1. The open literature 7-7-7 shaped hole geometry used for this study was developed by Schroeder and Thole [13] and is shown in Figure 2. The holes were rotated 45° about the y -axis to impart the compound angle and thus have “shingled” exits that are not aligned with the z -axis. Also shown in Figure 2 is the location of the origin at the geometric centerline of the hole. For compound angle holes fed by an internal crossflow, the direction of the crossflow is an important parameter. For the purposes of this study, the term “in-line crossflow” will refer to crossflow directed in-line with the span-wise direction of injection and “counter crossflow” will refer to crossflow in the opposite direction. A single row of eight holes was machined into a low conductivity polyurethane coupon ($k = 0.044 \text{ W/m}\cdot\text{K}$). The hole metering diameter was $d = 5 \text{ mm}$ and the hole pitch was $p/d = 6.25$.

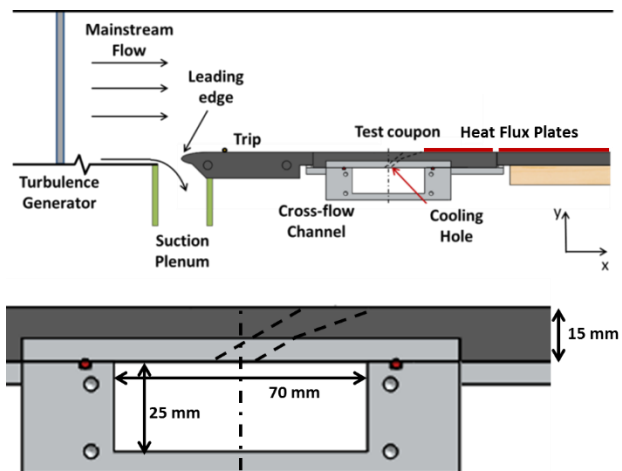


Figure 1: Schematic of test section and coolant channel

Table 1: Mainstream Parameters

Parameter	Value
Cooling Hole Diameter, d	5.0 mm
Mainstream Temp, T_∞	310 K
Mainstream Velocity, U_∞	25 m/s
Mainstream Turbulence Intensity, T_u	4.8%
Turbulence Integral Length Scale, Λ_x/d	2.0
Approach Boundary Layer Thickness, δ/d	2.3
Boundary Layer Displacement Thickness, δ^*/d	0.29
Boundary Layer Momentum Thickness, θ/d	0.22
Boundary Layer Shape Factor, H	1.33
Approach Reynolds Number, Re_d	7,500

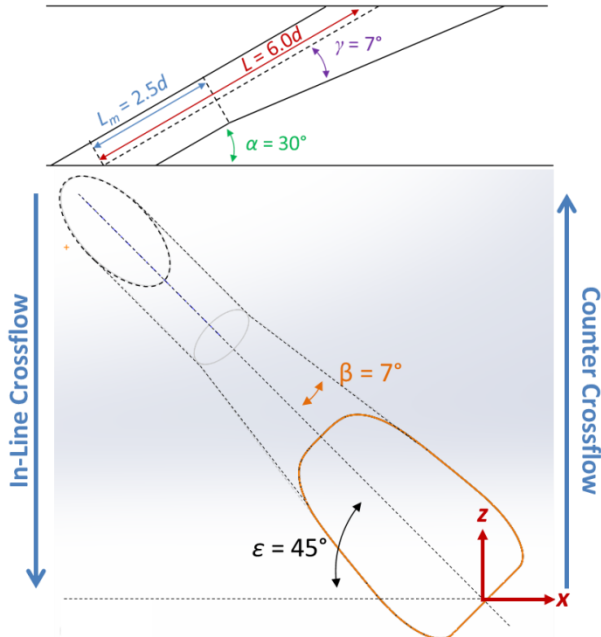


Figure 2: Compound angle 7-7-7 film cooling hole geometry

Table 2: Experimental Conditions

Parameter	Range Tested
$DR = \rho_j/\rho_\infty$	1.2
$VR = U_j/U_\infty$	0.2 - 1.7
$VR_c = U_c/U_\infty$	0.2 - 0.6
$VR_i = U_i/U_j$	0.1 - 3.3
$M = \rho_\infty U_\infty / \rho_j U_j$	0.2 - 2.0
$Re_c = \rho_c U_c d_H / \mu_c$	15,000 - 45,000
r_x	2 - 48%

Experiments were performed at a density ratio of $DR = 1.2$. In Part I of the paper [8], it was found that for axial shaped holes, density ratio had a measurable, but weak effect on adiabatic effectiveness and that all of the observed trends at an engine-relevant $DR = 1.8$ were preserved at $DR = 1.2$. Table 2 shows the experimental flow conditions tested in this study. Note that the extraction ratio, r_x , was the percentage of flow into the channel that was extracted as film cooling. An experiment with holes blocked off showed that there was no measurable effect of extraction ratio on film cooling effectiveness.

MEASUREMENT TECHNIQUES

Infrared (IR) thermography was used to measure the temperature of the test surface up to $40d$ downstream of the film cooling holes for the center four holes. Optical access was provided for a FLIR model A655sc IR camera through a zinc selenide window mounted on top of the test section. The surface was painted with a flat black paint to ensure uniform emissivity. The camera was calibrated *in situ* against Type-E surface thermocouples mounted on copper plates and placed on the test surface. During testing, the tunnel was allowed to reach steady state before measurements were made.

Two 0.025 mm stainless steel heat flux plates were adhered to the test surface. Due to the modular assembly of the test section, two heat flux plates were used – one on the test coupon itself ($x/d < 15$) and one on the downstream run-out plate ($x/d > 15$) – with a small gap between the two heat flux plates (see Figure 1). The plates were connected to separate power supplies which provided a constant heat flux of $q'' = 1.7 \text{ kW/m}^2$ to the surface. The heat fluxes of the two plates were held to within 1% of each other.

A pitot-static probe mounted downstream of the leading edge measured the mainstream velocity, U_∞ . Two type-E thermocouples installed near the test section inlet measured T_∞ . The coolant temperature was calculated as the average of two thermocouples installed at the inlet and outlet of the coolant channel. The pressure in the channel, used to measure discharge coefficients, was likewise computed as the average of the channel inlet and outlet pressures. The mass flow rate of coolant through the film cooling holes was calculated as the difference between the measured mass flow rates into and out of the channel. An orifice plate installed to ASME specifications measured the inlet mass flow rate, and a Venturi meter, calibrated against the inlet orifice meter, measured outlet mass flow rate.

DATA ANALYSIS

Discharge Coefficients

The discharge coefficients through the film cooling holes were calculated using the following equation from Gritsch *et al* [14]:

$$C_D = \frac{\dot{m}}{\frac{4}{\gamma} d^2 p_{tc} \left(\frac{p_\infty}{p_{tc}} \right)^{(\gamma+1)/2\gamma} \sqrt{\frac{2\gamma}{(\gamma-1)} R T_{tc} \left(\left(\frac{p_{tc}}{p_\infty} \right)^{(\gamma-1)/\gamma} - 1 \right)}} \quad (7)$$

Effectiveness and Heat Transfer Augmentation

A finite element method was used to correct for conduction in the test surface by predicting the heat flux required to produce the measured temperature distribution. T_{aw} was then calculated as:

$$T_{aw} = T_{measured} - \frac{q''}{h_f} \quad (8)$$

where q'' was predicted using the finite element solver and h_f was assumed to equal h_0 , which was predicted using correlations for heat transfer from a turbulent boundary layer on a flat plate. More details about this method can be found in [15].

A similar process was used to compute heat transfer augmentation. Conduction and radiation corrections were applied to the measured heat flux to the plate. The resultant heat flux was then used to determine the heat transfer coefficient:

$$h_f = \frac{q''}{T_{measured} - T_{aw}} \quad (9)$$

where T_{aw} was the adiabatic wall temperature with the heat flux plate turned off. The heat transfer coefficient without film cooling, h_0 , was similarly determined, using a measured wall temperature without film cooling and with the heat flux plate off as the driving temperature into the surface in order to correct out any effect of the cold thermal boundary that developed over the cold upstream test coupon.

Note that the initial calculation of T_{aw} involved the assumption that $h_f/h_0 = 1.0$. The calculated value of h_f/h_0 could then be used to correct that assumption. However, using h_f instead of h_0 to correct the measured temperature resulted in a negligible difference in laterally averaged effectiveness.

Jet Characteristic Parameters

Because crossflow is expected to alter the shape of the film cooling effectiveness profiles for film cooling holes, three jet characteristic parameters were examined: jet centerline effectiveness, η_{CL} , and location $(z/d)_{CL}$, and jet width, W . These parameters were computed as indicated by Figure 3. Note that the centerline effectiveness is not the effectiveness at the geometric centerline of the hole, but the highest effectiveness at a given streamwise location. The positive z direction was arbitrarily defined in the opposite direction of the holes. Thus, it is expected for compound angle holes, that $(z/d)_{CL}$ will be a negative value. The jet width was defined as the distance between the points on either side of $(z/d)_{CL}$ where $\eta = 0.5\eta_{CL}$.

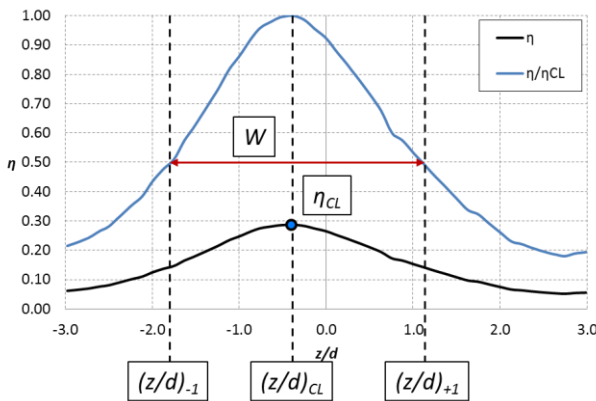


Figure 3: Jet characteristic parameters – sample η profile at $x/d = 10$

Predicted Overall Effectiveness

The one-dimensional model given in Eqn. 4 was used to predict overall effectiveness. This predicted value combines the effects of adiabatic effectiveness, heat transfer augmentation, and internal cooling. Gnielinski's formula was used to predict the internal heat transfer coefficient:

$$Nu_D = \frac{h_c d_H}{k_c} = \frac{(f/8)(Re_c - 1000)Pr}{1 + 12.7(f/8)^{1/2}(Pr^{2/3} - 1)} \quad (10)$$

$$f = (0.79 \ln(Re_c) - 1.64)^{-2} \quad (11)$$

The coolant warming factor was assumed to be $\chi = 0.9$ to account for warming of the coolant within the hole. An analysis performed by Dyson *et al* [16] estimated that the Biot number around an engine scale turbine airfoil ranges from $Bi = 0.1-1.0$. A target value of $Bi = 0.8$ was used to choose a constant wall thermal conductivity of $k = 1.0 \text{ W/m}\cdot\text{K}$ for the purposes of this analysis. This prediction is not expected to match engine overall effectiveness, rather, it quantifies the sum effect of changing VR_c .

REPEATABILITY AND UNCERTAINTY

Test-to-test uncertainty was confirmed by measuring adiabatic effectiveness in separate experiments. Two experiments run over a month apart agreed within ± 0.01 in η for multiple conditions. These measurements were made at different mainstream temperatures, necessitating different IR camera calibrations, so the repeatability exceeded the estimated precision uncertainty.

Uncertainty of measurements made in this study was estimated using the sequential perturbation method of Moffat *et al* [17]. The precision uncertainty of η was estimated to be $\delta\eta_p = \pm 0.005$, due to the uncertainty in mainstream temperature and flow rate. The bias uncertainty was estimated to be $\delta\eta_b = \pm 0.016$ and was primarily a result of uncertainty in the IR calibration. Heat transfer coefficient augmentation was estimated to have a precision uncertainty of $\delta(h_f/h_0)_p = \pm 0.008$ and a bias uncertainty of $\delta(h_f/h_0)_b = \pm 0.10$. The main source of uncertainty was the calculated T_{aw} used to determine h_0 . The bias and precision uncertainties of velocity ratio were $\delta(VR)_b = \pm 0.03$ and $\delta(VR)_p = \pm 0.010$ respectively. The bias and precision uncertainties of the crossflow velocity ratio were $\delta(VR_c)_b = \pm 0.005$ and $\delta(VR_c)_p = \pm 0.001$ respectively.

RESULTS AND DISCUSSION

Discharge coefficients, adiabatic effectiveness, and heat transfer coefficient augmentation were measured for a single row of compound angle 7-7-7 shaped film cooling holes fed by an internal crossflow. The crossflow-to-mainstream velocity ratio was varied from $VR_c = 0.2-0.6$ and the jet-to-mainstream velocity ratio was varied from $VR = 0.2-1.7$. Two crossflow directions were tested: in-line with and counter to the spanwise direction of coolant injection. This study presents the first measurements of varying crossflow velocity for compound angle shaped film cooling holes.

DISCHARGE COEFFICIENTS

The discharge coefficient of flow through a film cooling hole characterizes the losses through the hole relative to an ideal flow. These losses are expected to be the summation of losses at the hole inlet, in the hole itself, and due to interaction with the overflowing mainstream. In Part I of this paper [8], C_d was found to scale well with the ratio of the jet-to-crossflow velocity, $U_j/U_c = 1/VR_i$, with the exception of $VR_c = 0.2$. The same trend was observed for the compound angle holes of this study. Figure 4 shows the measured discharge coefficients for all conditions

tested scaled with (a) pressure ratio, and (b) U_j/U_c . As expected, the in-line crossflow had a higher discharge coefficient, and therefore fewer losses, than the counter crossflow due to the favorable direction of crossflow feeding the holes. When scaled with pressure ratio, the counter crossflow reduced C_d with increasing VR_c , due to the increased difficulty of flow turning into the holes. This effect was not observed for in-line crossflow. C_d collapsed for each flow direction when scaled with U_j/U_c , indicating that losses were strongly influenced by hole inlet effects. The exception to the trend occurred at $VR_c = 0.2$, where C_d was lower than the rest of the conditions for both flow directions. This exception was expected given that scaling with U_j/U_c is not expected to hold for plenum conditions ($VR_c = 0$, $U_j/U_c = \infty$) and therefore must break down at low VR_c . It is also worth noting that the in-line crossflow discharge coefficients experienced a maximum at $U_j/U_c \approx 1.5$, possibly because that velocity ratio was more favorable to turning of the flow into the holes.

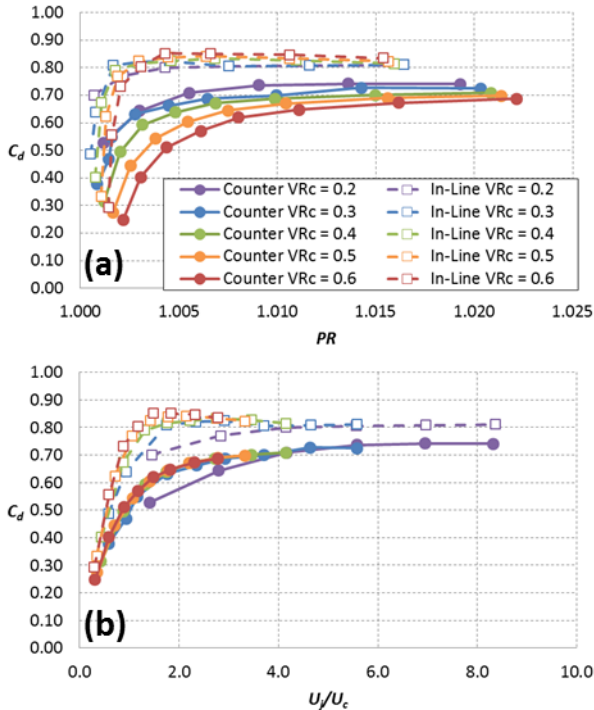


Figure 4: Discharge coefficients for all conditions scaled with (a) PR and (b) U_j/U_c

ADIABATIC EFFECTIVENESS

There are no previous studies of the effect of increasing VR_c on adiabatic effectiveness from compound angle shaped holes. Dittmar *et al* [11] found that for wide angle ($\beta = 14^\circ$) fan-shaped holes, holes fed by in-line crossflow were substantially more effective than those fed by counter crossflow. However, that study was performed for a different film cooling geometry than the one tested in this study and at an unspecified VR_c .

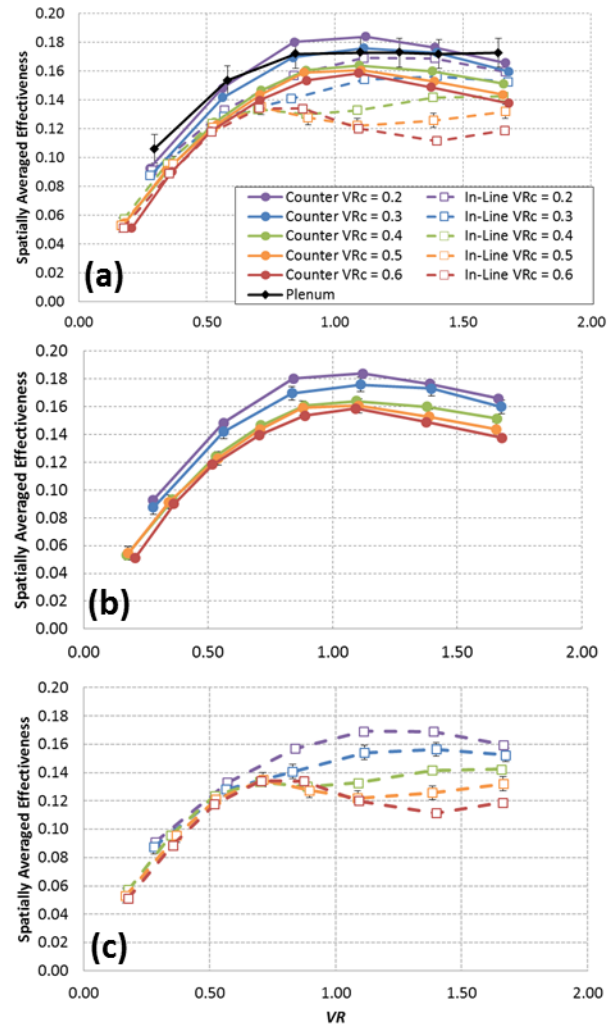


Figure 5: Spatially averaged effectiveness from $x/d = 5-20$ for: (a) all conditions (plenum data from [18]), (b) counter crossflow, and (c) in-line crossflow

It was found that crossflow direction and magnitude strongly affected the effectiveness of 7-7-7 compound angle shaped holes at high injection rates ($VR > 0.8$). Figure 5 (a) plots spatially averaged η for all conditions tested, averaged over three hole pitches and from $x/d = 5$ to 20. Unlike Dittmar *et al* [11], the counter crossflow resulted in higher effectiveness than the in-line crossflow, especially for $VR_c \geq 0.4$ and $VR > 0.8$. To improve readability, Figure 5 (b) and (c) separately plot the spatially averaged effectiveness for counter and in-line crossflow respectively. For both flow directions, increasing VR_c decreased the effectiveness, especially at higher injection rates. For the counter crossflow case, most of this reduction in effectiveness due to increasing crossflow velocity occurred between $VR = 0.8-1.7$, while there was little effect of increasing crossflow from $VR_c = 0.3-0.8$. For in-line crossflow, a notable shift in how VR affected film cooling effectiveness occurred when VR_c was increased from 0.3 to 0.4. For all counter crossflow cases and for

in-line crossflow with $VR_c \leq 0.3$, the peak effectiveness occurred at around $VR = 1.1$ and declined with a further increase in VR . However, for in-line crossflow with $VR_c \geq 0.4$, there was a notable deviation from that trend. For these cases effectiveness peaked at $VR = 0.7$, and declined significantly at higher VR . However, the spatially averaged effectiveness later increased with increasing VR after its initial decline. This later increase in effectiveness suggests that the initial decrease in effectiveness after $VR = 0.7$ did not occur due to separation of the jet above the wall, which is the typical explanation for reduced film cooling effectiveness with increasing injection rate. Figure 5 (a) also plots the spatially averaged η for a baseline plenum condition measured by [18], which was within uncertainty of the crossflow cases with the highest effectiveness. As for axial shaped holes, internal crossflow resulted in a reduction in effectiveness relative to the plenum case for all but the lowest VR_c .

Counter crossflow-fed holes were more effective due to the manner in which the coolant jets biased within the diffuser. Multiple studies have shown coolant biasing in the diffuser of axial shaped holes due to internal crossflow [5,6,7,8]. In Part I of this study, the degree of biasing was inversely related to the jet centerline effectiveness. For compound angle shaped holes, however, the direction of the biasing was critical as well. As shown in Figure 6, both counter and in-line crossflow caused the jet to bias toward the windward side of the diffuser relative to the internal crossflow, similar to the axial holes in Part I. Note that the contours of effectiveness are not corrected for conduction effects in order to show the observed profile in the film cooling holes. Because of the compound angle of the holes, the counter crossflow jets were more effective than the in-line jets because the coolant biased toward the upstream, rather than the downstream side of the diffuser relative to the mainstream flow direction. It is possible that the coolant jet on the upstream side of the diffuser blocked the mainstream flow from being ingested into the diffuser, while, for the in-line crossflow, the coolant biased toward the downstream edge of the diffuser allowed the mainstream gas to ingest into the upstream side of the diffuser and mix with the coolant. The difference in jet biasing also altered the jet trajectory. The mainstream turned the in-line jets in the downstream directions more effectively than it turned the counter jets.

Increasing crossflow velocity increased the bias within the diffuser. Figure 7 shows uncorrected contours of η at $VR = 1.11$, the injection rate corresponding to the peak effectiveness for most conditions tested. As VR_c was increased, the biasing in the hole for both flow directions became more severe. For in-line crossflow, as VR_c was increased to 0.4, the biasing became severe enough such that the hole was no longer filled out and the trajectory of the jet became aligned with the mainstream direction, and much less effective. The counter crossflow jets, however, maintained a similar trajectory as VR_c increased, although the centerline effectiveness was reduced with increasing VR_c , implying that the increased bias in the hole resulted in a more turbulent jet that more rapidly dispersed coolant away from the wall.

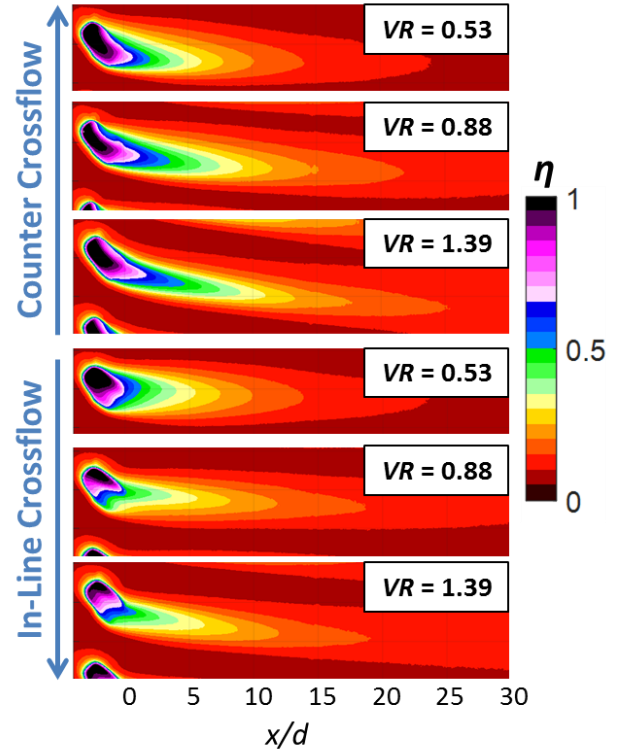


Figure 6: Contours of uncorrected η for $VR_c = 0.5$

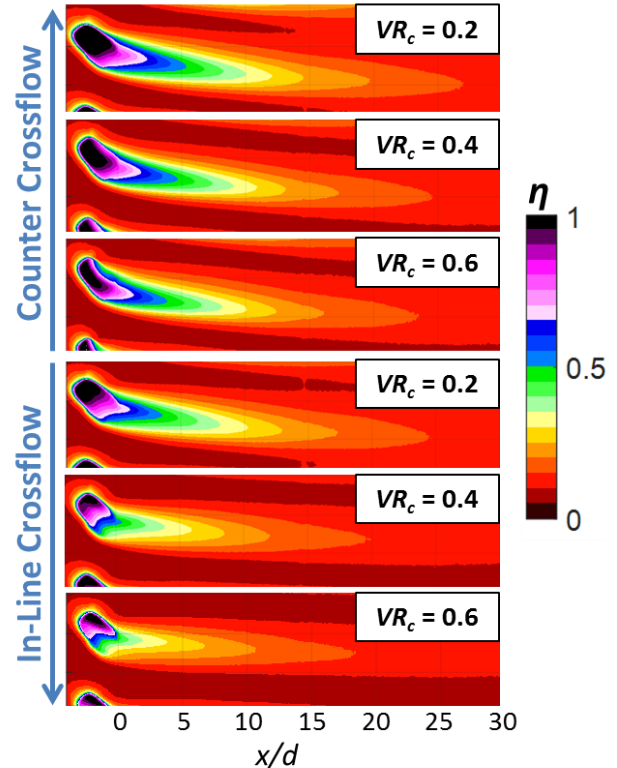


Figure 7: Contours of uncorrected η for $VR = 1.11$

JET CHARACTERISTICS

Three jet characteristics were computed from the measured adiabatic effectiveness profiles in order to better quantify the effect of crossflow on the film cooling performance: centerline effectiveness, η_{CL} , centerline location, $(z/d)_{CL}$, and jet width, W/d . In Part I of this study, these parameters all scaled with the hole inlet velocity ratio, $VR_i = U_c/U_j$ for axial 7-7-7 holes. However, for compound angle shaped holes, no single injection parameter was found to scale the data due to the added complication of compound angle injection.

Centerline Effectiveness

The centerline effectiveness scaled differently for counter and in-line crossflow because VR_c affected each crossflow direction differently. As was shown earlier, the degree of jet bias more strongly affected the effectiveness of the film cooling jets for in-line crossflow than it did for counter crossflow. For this reason, η_{CL} scaled well with VR_i for in-line crossflow, but not for counter crossflow. This result can be seen in Figure 8. The average centerline effectiveness for in-line crossflow had a local minimum at $VR_i = 0.4$ and otherwise tended to decrease with increasing VR_i . This scaling broke down at $VR < 0.4$, as evidenced by points with $\eta_{CL} < 0.15$ departing from the trend of the rest of the data. The shape of the curve for in-line crossflow was remarkably similar to that for the axial holes as shown in Figure 8 (b). The two curves fell nearly on top of each other, both had a local minimum at $VR_i = 0.4$, and the departures from the curves due to low VR were similar. For the axial holes, the minimum at $VR_i = 0.4$ corresponded with a maximum in jet bias. Similarly for in-line crossflow, movement of the bias toward the downstream side of the diffuser was associated with a severe degradation of effectiveness.

On the other hand, the average centerline effectiveness from counter crossflow-fed compound angle holes did not scale well with VR_i , as can be seen in Figure 8 (c). Although VR_c certainly affected biasing in the diffuser for counter crossflow, as was shown in Figure 7, VR_i was not sufficient to scale centerline effectiveness for this condition. Figure 9 (a) shows the scaling of η_{CL} with VR for counter crossflow. Similar to spatially averaged η , average η_{CL} tended to decrease with increasing VR_c . Figure 9 (b) shows the results of an attempt to scale η_{CL} using both VR and VR_c . It was found that $\eta_{CL} VR_c^{0.15}$ scaled well with VR , taking into account both the effect of crossflow at the hole inlet as well as the interaction with the mainstream. This result implies that increased VR_c resulted in increased turbulence generation in the hole and therefore increased dispersion of the jet above the surface, which scales with VR_c . The effectiveness however was most strongly influenced by the jet-mainstream interaction, which scales with VR . The scaling in Figure 9 (b) only holds for η_{CL} for these holes averaged over $x/d = 5-20$ and is thus limited in application. However, it provides useful insight into how flow physics at the inlet and exit of the hole combine to affect film cooling effectiveness.

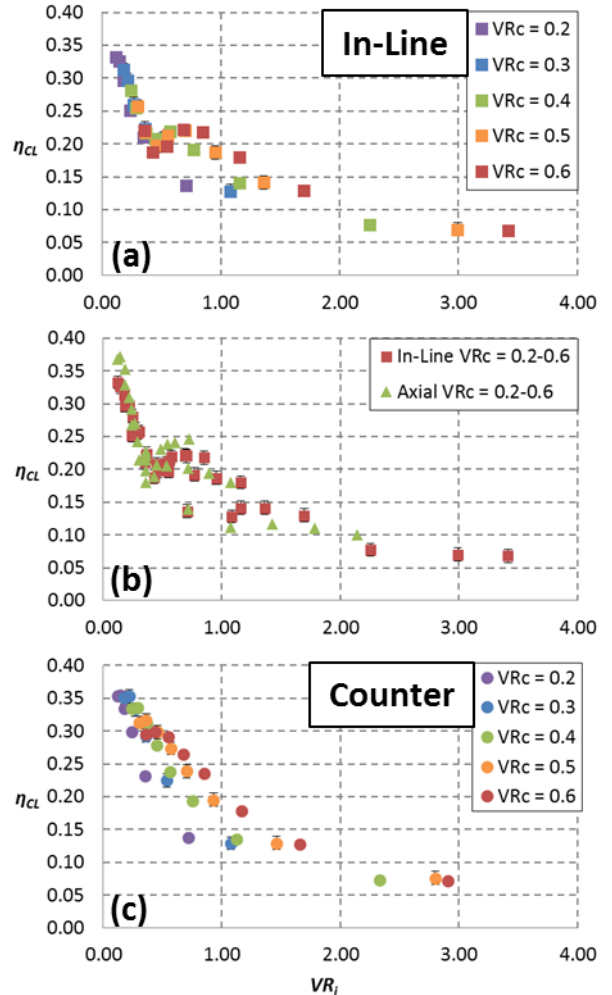


Figure 8: η_{CL} averaged from $x/d = 5-20$ scaled with VR_i : (a) in-line crossflow (b) in-line crossflow and axial holes, (c) counter crossflow

Centerline effectiveness for in-line and counter crossflow are compared using the scaling with VR and $\eta_{CL} VR_c^{0.15}$ in Figure 9 (c). The scaling works well for both crossflow directions for $VR < 0.8$ but breaks down for in-line crossflow at higher VR . The degradation in η_{CL} for the in-line crossflow condition shows the detrimental effects of biasing toward the downstream side of the hole relative to biasing toward the upstream side of the hole.

Centerline Location

Due to the span-wise component of injection the average jet centerline location was primarily a function of jet-to-mainstream velocity ratio, especially for counter crossflow, as shown by Figure 10 (a). This figure shows that the movement of the jet in the spanwise direction was dominated by the compound angle injection and was minimally influenced by the crossflow velocity at the hole inlet. Figure 10 (b) compares the centerline location for in-line flow to that of counter crossflow. Except at the lowest VR , the in-line crossflow jets had less lateral

movement than the counter crossflow jets. For $VR > 1.0$, the in-line jets had decreased jet movement with increasing VR_c , likely a result of the increased bias toward the downstream side of the diffuser.

Jet Width

Similarly to the jet centerline location, the jet width was predominantly a function of VR , as shown in Figure 11 (a) and (b). W/d collapsed very well for counter crossflow and for in-line crossflow for $VR < 1.0$. However, for $VR_c \geq 0.4$ and $VR > 1.0$, the width of the jets increased with increasing VR_c . The increased width of the jet in this case likely represents an increase in dispersal of the coolant. These wider jets corresponded to conditions where the jet also experienced decreased lateral movement and centerline effectiveness.

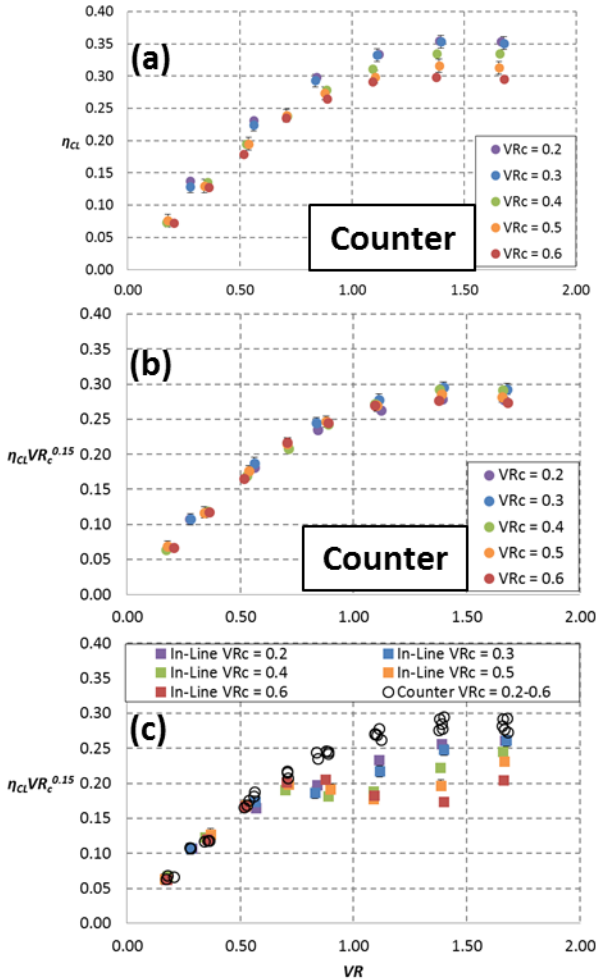


Figure 9: Average η_{CL} from $x/d = 5-20$ with different scaling parameters: (a) VR (b) and (c) VR and $VR_c^{0.15}$

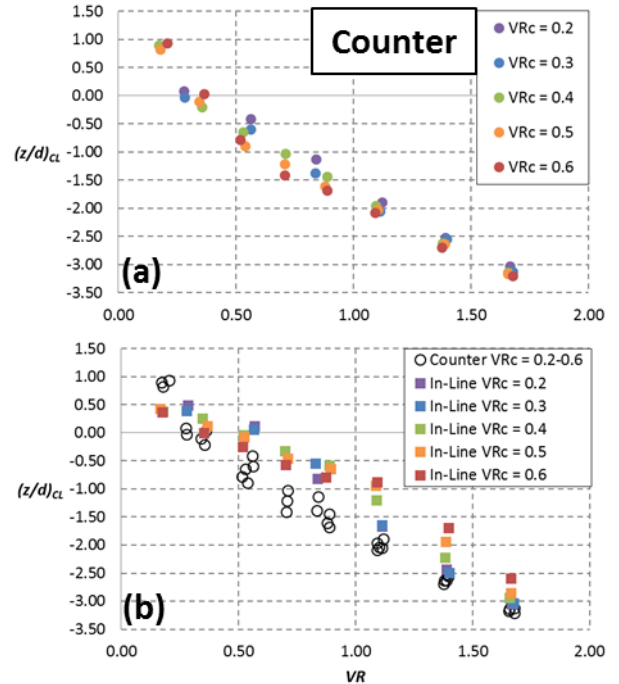


Figure 10: $(z/d)_{CL}$ averaged from $x/d = 5-20$: (a) counter crossflow (b) compared to in-line crossflow

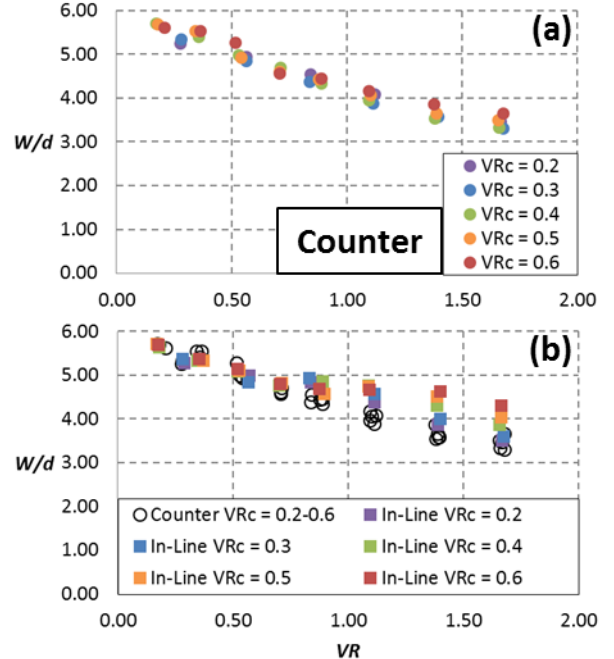


Figure 11: W/d averaged from $x/d = 5-20$: (a) counter crossflow (b) compared with in-line crossflow

HEAT TRANSFER COEFFICIENT AUGMENTATION

For plenum-fed holes, h_f/h_0 has been shown to be greater for compound angle shaped holes than for axial holes [3,4]. Compound angle injection causes the jets to block the mainstream, resulting in the development of a vortex on the downstream side of the jet that propagates downstream, causing a streak of enhanced heat transfer augmentation on that side of the jet. The same effect was observed for holes fed by internal crossflow. Figure 12 shows lateral profiles of η/η_{CL} and $h_{f,norm}$, which is defined as:

$$h_{f,norm} = \frac{h_f - h_0}{h_{f,peak} - h_0} \quad (12)$$

where $h_{f,peak}$ is the peak value of h_f at a given spanwise location. Note that $h_{f,norm} = 0$ corresponds to $h_f/h_0 = 1$. This scaling is useful to evaluate the relative shapes of the h_f/h_0 profiles and to show how the peak effectiveness lines up with the peak heat transfer augmentation. As expected, the peak augmentation occurred on the downstream (positive z/d) side of the jet. Note also that a second peak in heat transfer augmentation occurred under the positive z/d side of the jet that increased in magnitude relative to the primary peak augmentation as the velocity ratio increased from $VR = 1.11$ to 1.67 . This second peak was likely the result of turbulence within the jet, which is expected to increase with increasing VR . The magnitude of this second peak relative to the primary peak augmentation was also higher for counter crossflow than it was for in-line crossflow. This result was also unsurprising because the counter crossflow likely had increased in-hole turbulence generation due to the sharper turning angle at the hole inlet and the accompanying larger separation region. These trends – increased heat transfer augmentation under the jet for higher VR and for counter crossflow – were consistent for all conditions tested.

The location of the peak heat transfer augmentation was shown to be predominantly a function of injection rate. Figure 13 (a) plots the lateral location of peak heat transfer augmentation for in-line crossflow. VR_c had little effect, especially at higher VR . Lateral movement of the peak h_f/h_0 in the negative z/d direction increased with increasing VR . Interestingly, the peak location moved in the positive z/d direction for $VR = 0.56$, even though $(z/d)_{CL}$ based on effectiveness moved in the opposite direction, as shown in Figure 13 (b). For higher VR , the peak h_f/h_0 location moved in the same directions as the jets, although the separation between the jet and the peak h_f/h_0 location increased going downstream. Similar results were seen for counter crossflow and other crossflow velocity ratios.

Similarly, the laterally and spatially averaged augmentation was primarily dependent on VR . Figure 14 plots laterally and spatially averaged $h_{f,norm}$ for all conditions tested, using the peak local value of h_f as $h_{f,peak}$. Note that the gap in the data from $x/d = 14-17$ occurred where there was a seam between the test coupon and the downstream runout plate where there was no heat flux plate. At the lowest and highest injection rate ($VR = 0.56$ and 1.67) there was little variation in $h_{f,norm}$ due to crossflow

effects. In general, $h_{f,norm}$ increased with increasing VR as expected – increasing the film cooling rate increases the blockage of the mainstream, resulting in stronger turbulence structures downstream of the hole. The increase in $h_{f,norm}$ due to VR occurred in both the near-hole and downstream regions.

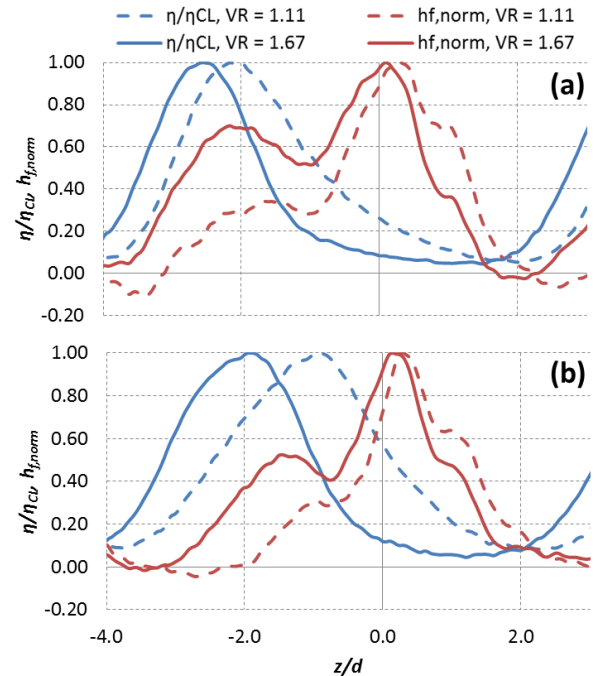


Figure 12: Lateral profiles of $h_{f,norm}$ and η/η_{CL} for $VR_c = 0.6$, $x/d = 5$ for (a) counter and (b) in-line crossflow

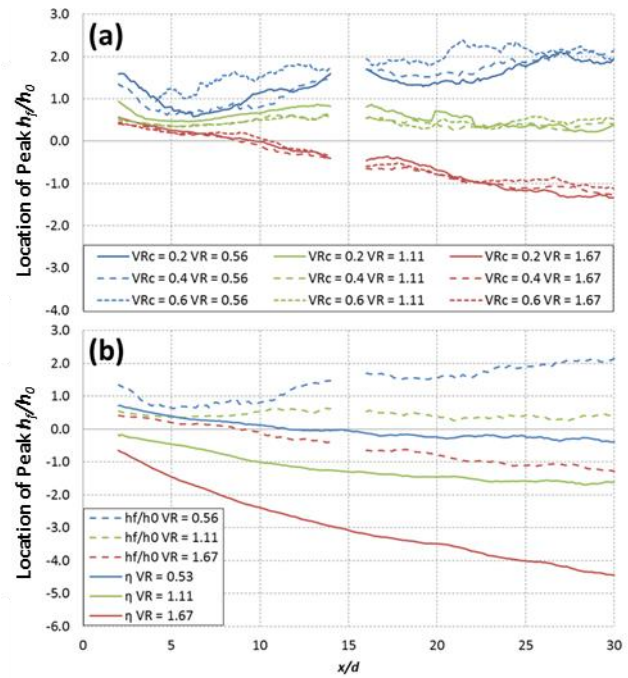


Figure 13: (a) Locations of peak h_f/h_0 for in-line crossflow
(b) compared with $(z/d)_{CL}$ at $VR_c = 0.4$

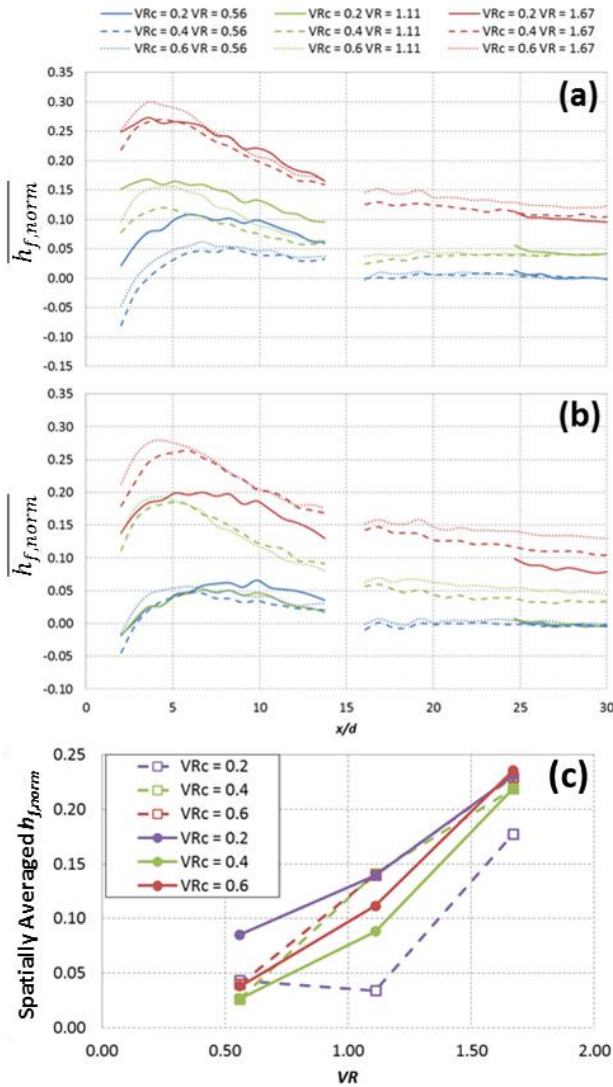


Figure 14: Laterally averaged $\bar{h}_{f,norm}$ for (a) counter and (b) in-line crossflow. (c) Spatially averaged $\bar{h}_{f,norm}$ for $x/d = 5-14$

The effect of internal crossflow on $\bar{h}_{f,norm}$ was mostly limited to $VR = 1.11$, where there was considerable variation due to both crossflow direction and magnitude. For counter crossflow, $\bar{h}_{f,norm}$ was slightly lower at $VR_c = 0.4$ than for $VR_c = 0.2$ or 0.6 . For in-line flow, $\bar{h}_{f,norm}$ was near zero at $VR_c = 0.2$ and then increased significantly when VR_c increased to 0.4 . This increase corresponded to the reduction in effectiveness and jet movement and the increase in jet width observed at higher VR_c for in-line crossflow. This result is somewhat surprising, given that the in-line jets tended to have less lateral movement than the counter crossflow jets, and thus would be expected to have reduced mainstream blockage.

PREDICTION OF OVERALL EFFECTIVENESS

Overall cooling effectiveness was predicted using the one-dimensional model given in Equation 4. This prediction can be

used to show the relative importance of internal cooling, adiabatic effectiveness, and heat transfer coefficient augmentation relative to each other. The results presented thus far have shown that increasing VR_c can affect both η and \bar{h}_f/h_0 , illustrating the complexity of turbine cooling and the need to understand of how internal coolant feed can affect overall film cooling effectiveness in a number of ways. Figure 15 shows the result of applying this model to the measured η and \bar{h}_f/h_0 at $VR = 1.11$, which was the condition with highest η for most crossflow conditions. The predicted overall cooling effectiveness was primarily driven by the internal cooling, as evidenced by increased φ_p with increasing VR_c , despite decreasing η . The increased η and reduced \bar{h}_f/h_0 combined to give counter crossflow higher φ_p at $VR_c = 0.4$ and 0.6 relative to in-line crossflow.

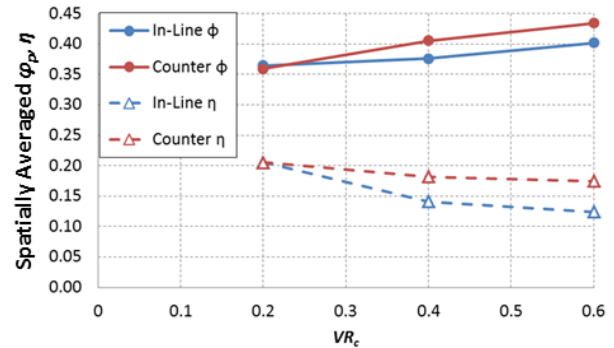


Figure 15: Predicted φ and measured η for $VR = 1.11$, spatially averaged over $x/d = 5-14$

CONCLUSIONS

Adiabatic effectiveness, heat transfer coefficient augmentation, and discharge coefficients were measured for a single row of compound angle 7-7-7 diffused exit film cooling holes. The holes were fed by an internal crossflow directed counter to, and in-line with, the lateral direction of coolant holes. A range of channel-to-mainstream velocity ratios, $VR_c = 0.2-0.6$, and jet-to-mainstream velocity ratios, $VR = 0.2-1.7$, was tested. The important results from this study are as follows:

- The internal crossflow direction affected how the jets were biased within the diffuser. In-line crossflow caused a bias towards the downstream side of the diffuser and counter crossflow caused a bias towards the upstream side of the diffuser.
- For in-line crossflow, the bias towards the downstream side of the hole caused a severe degradation in film cooling effectiveness, a reduction in jet lateral movement, an increase in jet width, and an increase in heat transfer augmentation. This effect was observed for $VR_c > 0.4$.
- Most measured values tended to scale best with jet-to-mainstream velocity ratio, VR , including \bar{h}_f/h_0 , the effectiveness of counter crossflow-fed holes, jet lateral movement, and jet width. Other parameters, including

in-line crossflow centerline effectiveness and discharge coefficient scaled best with the inlet velocity ratio, $VR_i = U_c/U_j$. The differences in scaling demonstrate that the importance of flow at the inlet of the hole vary for both the crossflow orientation and for the different metrics examined in the study.

- The scaling of centerline effectiveness of in-line crossflow-fed holes with VR_i as well as the scaling of the discharge coefficients with U_j/U_c closely resembled the scaling with these parameters for axial holes.
- A one-dimensional model was used to predict overall cooling effectiveness. It was shown that the internal cooling had the strongest influence on overall effectiveness, while adiabatic effectiveness and heat transfer coefficient augmentation had a small but notable effect.

More work is needed to better understand these results. Specifically, thermal and flow field measurements above the surface of the wall in the near-hole region and perhaps within the hole could provide more insight on how jet bias in the diffuser affects film cooling effectiveness and heat transfer coefficient augmentation. Similarly, investigating more compound angle shaped hole geometries would show whether the effects observed in this study are geometry-dependent or more universal in nature.

ACKNOWLEDGMENTS

The authors are grateful for the continued financial and technical support from GE Aviation and GE Global Research.

REFERENCES

- [1] Bunker, R. S., 2005, "A Review of Shaped Hole Turbine Film-Cooling Technology," *J. Heat Transfer*, Vol. 127, pp. 441-453.
- [2] Taslim, M. E. and Khanicheh, A., 2005, "Film Effectiveness Downstream of an Row of Compound Angle Holes," *J. Heat Transfer*, **127**, pp. 434-440.
- [3] Bell, C. M., Hamakawa, H., and Ligrani, P. M., 2000, "Film Cooling from Shaped Holes," *J. Heat Transfer*, **122**, pp. 224-232.
- [4] Ganzert, W., Hildebrandt, T., and Fottner, L., 2000, "Systematic Experimental and Numerical Investigations on the Aerothermodynamics of a Film Cooled Turbine Cascade with Variation of the Cooling Hole Shape, Part I: Experimental Approach," ASME Paper No. 2000-GT-295.
- [5] Gritsch, M., Schulz, A., and Wittig, S., 2003, "Effect of Internal Coolant Crossflow on the Effectiveness of Shaped Film-Cooling Holes," *J. Turbomach.*, **125**, pp. 547-554.
- [6] Saumweber, C. and Schulz, A., 2012, "Effect of Geometry Variations on the Cooling Performance of Fan-Shaped Cooling Holes," *J. Turbomach.*, **134**, p.061008.
- [7] Wilkes, E. K., Anderson, J. B., McClintic, J. W., and Bogard, D. G., 2016, "An Investigation of Turbine Film Cooling Effectiveness with Shaped Holes and Internal Cross-Flow with Varying Operational Parameters," ASME Paper No. GT2016-56162.
- [8] McClintic, J. W., Anderson, J. B., Bogard, D. G., Dyson, T. E., and Webster, Z., "Effect of Internal Crossflow Velocity on Film Cooling Effectiveness – Part I: Axial Shaped Holes," ASME Paper No. GT2017-64616.
- [9] McClintic, J. W., Klavetter, S. R., Winka, J. R., Anderson, J. B., Bogard, D. G., Dees, J. E., Laskowski, G. M., and Briggs, R., 2015, "The Effect of Internal Crossflow on the Adiabatic Effectiveness of Compound Angle Film Cooling Holes," *J. Turbomach.*, **137**, p.071006.
- [10] Stratton, Z. T., Shih, T. I., Laskowski, G. M., Barr, B., and Briggs, R., 2015, "Effects of Crossflow in an Internal-Cooling Channel on Film Cooling of a Flat Plate Through Compound-Angle Holes," ASME Paper No. GT2015-42771.
- [11] Dittmar, J., Schulz, A., and Wittig, S., 2002, "Assessment of Various Film Cooling Configurations Including Shaped and Compound Angle Holes Based on Large Scale Experiments," ASME Paper No. GT-2002-30176.
- [12] Anderson, J. B., Wilkes, E. K., McClintic, J. W., and Bogard, D. G., "Effects of Freestream Mach Number, Reynolds Number, and Boundary Layer Thickness on Film Cooling Effectiveness of Shaped Holes," ASME Paper No. GT2016-56152.
- [13] Schroeder, R. P. and Thole, K. A., 2014, "Adiabatic Effectiveness Measurements for a Baseline Shaped Film Cooling Hole," ASME Paper No. GT2014-25992.
- [14] Gritsch, M., Saumweber, C., Schulz, A., Wittig, S., and Sharp, E., 2000, "Effect of Internal Coolant Crossflow Orientation on the Discharge Coefficient of Shaped Film-Cooling Holes," *J. Turbomach.*, **122**, pp. 146-152.
- [15] Klavetter, S. R., McClintic, J. W., Bogard, D. G., Dees, J. E., Laskowski, G. M., and Briggs, R., 2015, "The Effect of Rib Turbulators on Film Cooling Effectiveness of Round Compound Angle Holes Fed by an Internal Cross-Flow," ASME Paper No. GT2015-43947.
- [16] Dyson, T. E., McClintic, J. W., Bogard, D. G., and Bradshaw, S. D., 2013, "Adiabatic and Overall Effectiveness for a Fully Cooled Turbine Vane," ASME Paper No. GT2013-94928.
- [17] Moffat, R. J., 1985, "Using Uncertainty Analysis in the Planning of an Experiment," *J. Fluids Eng.*, Vol. 107, pp. 173-178.
- [18] Anderson, J. B., McClintic, J.W., Bogard, D. G., Dyson, T. E., and Webster, Z., 2017, "Freestream Flow Effects on Film Effectiveness and Heat Transfer Coefficeint Augmentation for Compound Angle Shaped Holes," ASME Paper No. GT2017-64853.